High PD-1/PD-L1 Checkpoint Interaction Infers Tumor Selection and Therapeutic Sensitivity to Anti-PD-1/PD-L1 Treatment

Lissete Sánchez-Magraner[1], James Miles[1,2,3,4], Claire L. Baker[2], Christopher J. Applebee[1,2,3], Dae-Jin Lee[5], Somaia Elsheikh[6], Shaimaa Lashin[6], Katriona Withers[2], Andrew G. Watts[7], Richard Parry[7], Christine Edmead[3,8], Jose Ignacio Lopez[9], Raj Mehta[10], Antoine Italiano[4], Stephen G. Ward[8], Peter J. Parker[11,12], and Banafshé Larijani[1,2,3]

ABSTRACT

Many cancers are termed immunoevasive due to expression of immunomodulatory ligands. Programmed death ligand-1 (PD-L1) and cluster of differentiation 80/86 (CD80/86) interact with their receptors, programmed death receptor-1 (PD-1) and cytotoxic T-lymphocyte antigen-4 (CTLA-4), respectively, on tumor-infiltrating leukocytes eliciting immunosuppression. Immunotherapies aimed at blocking these interactions are revolutionizing cancer treatments, albeit in an inadequately described patient subset. To address the issue of patient stratification for immune checkpoint intervention, we quantitatively imaged PD-1/PD-L1 interactions in tumor samples from patients, employing an assay that readily detects these intercellular protein–protein interactions in the less than or equal to 10 nm range. These analyses across multiple patient cohorts demonstrated the intercancer, interpatient, and intratumoral heterogeneity of interacting immune checkpoints. The PD-1/PD-L1 interaction was not correlated with clinical PD-L1 expression scores in malignant melanoma. Crucially, among anti-PD-1–treated patients with metastatic non–small cell lung cancer, those with lower PD-1/PD-L1 interaction had significantly worsened survival. It is surmised that within tumors selecting for an elevated level of PD-1/PD-L1 interaction, there is a greater dependence on this pathway for immune evasion and hence, they exhibit more impressive patient response to intervention.

Significance: Quantitation of immune checkpoint interaction by direct imaging demonstrates that immunotherapy-treated patients with metastatic NSCLC with a low extent of PD-1/PD-L1 interaction show significantly worse outcome.

Introduction

Disproportionate immune system activation can result in profound pathologies and there are therefore, regulatory mechanisms in place to maintain homeostasis (1). Interactions referred to as immune checkpoints are critical in this, avoiding immune cell–related collateral damage in pathogenic responses and in suppressing autoimmunity. Inhibitory receptors presented by immune cells, T cells in particular, include programmed death receptor-1 (PD-1) and cytotoxic T-lymphocyte antigen-4 (CTLA-4; refs. 2, 3). Cancers exploit these physiologic mechanisms to avoid immune attack by expressing inhibitory receptor cognate ligands, programmed death ligand-1 (PD-L1) and cluster of differentiation 80/86 (CD80/86; ref. 1). The CTLA-4 receptor is a homolog of the immune-activating CD28 receptor, both of which are found on T cells and possess CD80 and CD86 as ligand partners (4). CTLA-4, however, provides a higher affinity binding site for CD80/86 and interaction with CD80/86 inhibits cell proliferation and IL2 secretion by T cells. The PD-1 immune checkpoint limits later immune responses primarily in peripheral tissue by attenuating T-cell signaling downstream of the T-cell receptor (5).

There are a number of approved therapeutic mAbs designed to reinstate immune-mediated tumor destruction in immunogenic cancers, by inhibiting the aforementioned immune checkpoint interactions (6). In part, through the generation of neoantigens, immunogenicity is strong in non–small cell lung cancer (NSCLC), renal cell carcinomas (RCC), melanoma, classical Hodgkin lymphoma, head and neck squamous cell carcinoma, and urothelial carcinoma, all of which show varying degrees of response to immune checkpoint interventions (6–8). Notwithstanding some remarkable successes with immune checkpoint inhibitors, the majority of patients display primary or acquired resistance to treatment (9). There is, therefore,

[1]FASTBASE Solutions S.L, Astondo bidea, Derio, Spain. [2]Cell Biophysics Laboratory, Ikerbasque, Basque Foundation for Science, Research Centre for Experimental Marine Biology and Biotechnology (PiE) & Biophysics Institute (UPV/EHU, CSIC), University of the Basque Country, Leioa, Biscay, Spain. [3]Centre for Therapeutic Innovation, Cell Biophysics Laboratory, Department of Pharmacy and Pharmacology, & Department of Physics, University of Bath, Claverton Down, Bath, United Kingdom. [4]Early Phase Trials and Sarcoma, Institut Bergonié, Cours de l'Argonne, Bordeaux, France. [5]Basque Centre for Applied Mathematics, Bilbao, Bizkaia, Spain. [6]Department of Cellular Pathology, Queens Medical Centre, Nottingham, United Kingdom. [7]Bath ASU, Corsham, United Kingdom. [8]Leukocyte Biology Laboratory, Centre for Therapeutic Innovation & Department of Pharmacy and Pharmacology, University of Bath, Claverton Down, Bath, United Kingdom. [9]Department of Pathology, Cruces University Hospital, Biocruces Research Institute, Barakaldo, Bizkaia, Spain. [10]Apple Tree Partners, London, United Kingdom. [11]Protein Phosphorylation Laboratory, The Francis Crick Institute, London, United Kingdom. [12]School of Cancer and Pharmaceutical Sciences, King's College London, London, United Kingdom.

Note: Supplementary data for this article are available at Cancer Research Online (http://cancerres.aacrjournals.org/).

L. Sanchez-Magraner and J. Miles are joint first authors for this article.

Corresponding Authors: Banafshé Larijani, Centre for Therapeutic Innovation, University of Bath, Claverton Down, Bath, BA2 7AY, United Kingdom. Phone: 4412-2538-4040; E-mail: bl666@bath.ac.uk; and Peter J. Parker, Protein Phosphorylation Laboratory, The Francis Crick Institute, 1 Midland Road, London, NW1 1AT, United Kingdom. Phone: 4402-0379-61977; E-mail: peter.parker@crick.ac.uk

Cancer Res 2020;80:4244–57

doi: 10.1158/0008-5472.CAN-20-1117

an unmet clinical need to identify biomarkers that distinguish potential responders from nonresponders to ensure that nonresponders are not exposed to the side-effects of these drugs for no therapeutic benefit.

The development of different PD-L1 IHC diagnostics utilizing proprietary antibodies has resulted in four FDA-approved and CE-*in vitro* diagnostics–marked assays, each linked to a specific drug and scoring system (10). However, it has become clear that the expression of inhibitory ligands, namely PD-L1, is not an accurate diagnostic marker for use in predicting patient prognosis and response to treatment. A recent study observed that patients with NSCLC demonstrated an increase in response to the anti-PD-1 agent, pembrolizumab, in patients exhibiting a tumor proportion score greater than 50% (11). Nevertheless, the response reached only 41% (12). Moreover, a different study assessed the efficacy of PD-1 or PD-L1 inhibitors in different neoplasia (primarily lung cancer but also renal cancer and malignant melanoma) in PD-L1–negative and PD-L1–positive cancers. Critically, benefit was seen in patients within the PD-L1–negative group, clearly exposing the failure of PD-L1 expression to determine which patients should receive immune checkpoint inhibitors (13).

As immune cell/tumor cell interplay via immune checkpoints is a prominent mechanism for tumor immune evasion and survival, checkpoint interaction status may present a key mechanism-based prognostic and/or predictive biomarker, replacing conventional protein expression readouts for stratifying patients to immune checkpoint interventions. To this end, we have developed and tested an imaging assay that provides a quantitative readout of immune checkpoint interaction between cells. iFRET (immune-FRET) employs a two-site, cell–cell amplified Förster resonance energy transfer (FRET) method, detected by fluorescence lifetime imaging microscopy (FRET/FLIM). Here, iFRET acts as a "chemical ruler," measuring cell–cell interactions in the range of 1–10 nm. Alternative assays have assessed the PD-1/PD-L1 signaling axis in both cell assays and patient tissue, however, these assays work at a distance greater than that of iFRET (Supplementary Fig. S1A). Work carried out by Giraldo and colleagues (2018), uses an imaging algorithm that determines when PD-1^+ and PD-$L1^+$ cells are within close proximity (≤20 μm) of each other. Such assays investigate distances that reflect proximity over interaction (14). Johnson and colleagues (2018), also utilized an automated quantitative analysis platform, which again maps cells based on PD-1 and PD-L1 expression profiles. In these assays, the colocalization of PD-1- and PD-L1–expressing cells (i.e., μm range) is assumed to be an interaction state (15). Here, the intrinsic distance constraints of iFRET informs on interaction states as receptor and ligand pairs within 1–10 nm of each other; distances exceeding 10 nm are considered to be non-interacting.

In this study, we have investigated the application of iFRET in formalin-fixed, paraffin-embedded (FFPE) patient tumor biopsies to assess checkpoint interaction, to understand the relationship of this to ligand expression, and to judge the predictive power of the data in respect of patient response to immune checkpoint interventions.

Materials and Methods

Pathology

Clear-cell RCC

Biopsies from patients with clear-cell RCC (ccRCC), diagnosed and treated at the Cruces University Hospital (Barakaldo, Bizkaia, Spain), were graded and staged within the study. All patients gave written informed consent for the potential use of their resected tumors for research. This study was approved by the Ethical and Scientific Committee (CEIC-Euskadi PI2015060). The International Society of Urological Pathology 2013 tumor grading system (16) was used to assign each sample using routine hematoxylin and eosin (H&E) staining. Tumors were graded and grouped as low (G1/2) and high (G3/4) grade for consistency. To assess PD-L1 expression, a multisite tumor sampling (MSTS) method was used, which samples more areas of a tumor with the aim of overcoming the problems of tissue heterogeneity (17). Samples were determined PD-L1 positive (>1%) or negative (<1%) using the Roche VENTANA PD-L1 (SP142) Assay.

Malignant melanoma

Cases of malignant melanoma used in this study were selected from all patients diagnosed with malignant melanoma between June 2003 and February 2017 at Nottingham University Hospital (Nottingham, England, United Kingdom). The main selection criterion was tumors having a Breslow thickness of >1 mm. Patients gave written informed consent for their specimens to be stored and used for research. Patient clinicopathologic data were obtained from Nottingham University Hospital PAS, WinPath, and NotIS databases. Data and specimens were anonymized by using only their designated laboratory case reference. Ethical approval (ACP0000174) was gained from the Nottingham Health Science Biobank Access Committee. A cohort of 176 primary malignant melanoma cases was used for iFRET analysis as tissue microarrays (TMA). Within the TMAs, each patient had one tumor sample. Supplementary Table S1 summarizes the clinical parameters of the 176 patients. Tumors were fully surgically excised and FFPE in tissue blocks. Tissue cores of 1-mm diameter were selected by studying H&E-stained sections most recently cut from the FFPE tissue block. The location of cores to remove from the tissue block was selected by scanning the slides and using Pannoramic Viewer Software (3DHisTech). Cores were removed from the FFPE tissue blocks using the TMA Grand Master (3DHisTech) and arrayed into new paraffin blocks.

Metastatic NSCLC

Biopsies from 60 metastatic NSCLC tumors were obtained during interventional radiology procedures from Institut Bergonié (Bordeaux, France; Supplementary Table S2). Thirty-six patients were male and 24 female with a median age of 63 years (range, 44–86 years). Performance status was defined with 50 patients given a performance status of ≤1 and 10 patients given a status of ≥1. Performance status is a measure of a patients' progress, with a grade of 0 being defined as fully active with the patient being able to carry on all predisease activities without restriction. A score of 1–3 indicates increasing severity of limitations to daily activities and self-care. A score of 4 is defined as completely disabled and 5 is defined as dead (18). The clinical outcome of 40 patients who were treated with either nivolumab ($n = 37$) or pembrolizumab ($n = 3$) was provided and used for Kaplan–Meier survival analysis. Patients' samples were collected between January 2014 and December 2017. This study was approved by the Institutional Review Board of Institut Bergonié (Bordeaux, France). Excised samples were FFPE in tissue blocks prior to being sliced and mounted on microscope slides. For iFRET analysis, three consecutive tissue slices of each patient's sample were provided. One slide for each patient sample was labeled with H&E and a trained pathologist (J.I. Lopez) identified tumorous areas within the sample.

Antibodies and reagents

Monoclonal antibodies, mouse anti-PD-1 (catalog no.: ab52587, clone number: NAT105), rabbit anti-PD-L1 (catalog no.: ab205921, clone number: 28–8), and mouse anti-CTLA-4 (catalog no.: ab19792, clone number: BNI3) were purchased from Abcam. Rabbit anti-CD80

(catalog no.: MBS2522916, clone number: MEM-233) was purchased from MyBioSource. The experimental antibody, J1201, which blocks PD-1/PD-L1 interactions was obtained from Promega. Ipilimumab, which blocks CTLA-4/CD80 interactions was also obtained from Promega. Pierce endogenous peroxidase suppressor (35000), Signal Amplification Kit (T20950), and Prolong Diamond Antifade Mount (P36970) were obtained from Thermo Fisher Scientific. AffiniPure F(ab′)2 fragment donkey anti-mouse IgG and peroxidase-conjugated AffiniPure F(ab′)2 fragment donkey anti-rabbit IgG were purchased from Jackson ImmunoResearch Laboratories. ATTO 488 NHS ester was purchased and conjugated to the AffiniPure F(ab′)2 IgG as described by Veeriah and colleagues (2014; ref. 19). Millicell 8-well plates (PEZGS0816) were purchased from Merck.

Time-resolved amplified iFRET detected by FLIM

iFRET relies on a two-site labeling assay, which is illustrated in Supplementary Fig. S1B. Briefly, two primary antibodies are used to detect the receptor and ligand, respectively. These antibodies are then labeled with Fab fragments conjugated to the donor chromophore ATTO488 (for the receptor) and horseradish peroxidase (HRP) for the ligand. Tyramide signal amplification is then used to label HRP with the acceptor chromophore, ALEXA594 (Supplementary Fig. S2A). The conjugation of the chromophores to Fab fragments, which bind to the two primary antibodies, allows the critical FRET distance of 10 nm or less to be maintained and provides the appropriate tool for measuring cell–cell interactions. It should be noted that additional stains, such as DAPI, cannot be added to iFRET samples as they disrupt the ability of ATTO488 and ALEXA594 to undergo FRET. Using a semi-automated, high-throughput mfFLIM (FASTBASE Solutions S. L; Supplementary Fig. S2B), a mapping file was created, which mapped each region of interest according to its position on the slide (Veeriah and colleagues, 2014; ref. 19; Supplementary Materials and Methods). Phase lifetimes, average intensities, and lifetime images were calculated automatically and translated to an excel spreadsheet. A decrease of donor lifetime (τD) in the presence of the acceptor chromophore (τDA) is indicative of resonance energy transfer. FRET efficiency (E_f %) values were calculated using the following equation, where τD and τDA are the lifetimes of the donor in the absence and presence of the acceptor, respectively.

$$Ef(\%) = \left[1 - \left(\frac{\tau DA}{\tau D}\right)\right] \times 100$$

Because of the Förster radius (R_0) of the chromophore pair ATTO488 and Alexa594, the minimum distance that can exist between the chromophores is 5.83 nm (Supplementary Fig. S2C; Supplementary Materials and Methods). At this distance, energy transfer is maximal and yields a FRET efficiency of 50%.

iFRET assay for PD-1/PD-L1 interaction in cell culture

The commercially validated Promega Blockade Bioassay, originally designed to measure the antibody blockade of PD-1/PD-L1 and CTLA-4/CD80 interaction by luminescence, was adapted for an iFRET protocol with the aim of verifying the technique for detecting intercellular interaction of these ligand/receptor pairs. Cells were obtained from the Promega Blockade Bioassay and screened for *Mycoplasma* prior to dispatch. These cells were thawed and directly used in this assay only. PD-L1–expressing CHO-K1 cells were seeded onto Millicell 8-well plates and were incubated at 37°C with 5% CO_2 for 16 hours. The experimental blocking antibody, J1201 (anti-PD-1), was added to four wells at 25 μg/mL final concentration to inhibit receptor–ligand interaction. PD-1–expressing Jurkat cells were subsequently seeded in all wells and the plates were incubated for 20 hours at 37°C with 5% CO_2. The unbound cells were removed and the plates were washed three times for 5 minutes with PBS before being fixed with 4% paraformaldehyde (PFA) for 12 minutes. The PFA was then removed and the plates were washed three times for 5 minutes with PBS. All samples were incubated with endogenous peroxidase suppressor for 30 minutes at room temperature before being washed with PBS. They were subsequently incubated with 1% (10 mg/mL) BSA for 1 hour at room temperature before further washing with PBS three times.

Primary antibody staining was carried out by adding mouse anti-PD-1 (1:100 in BSA), the donor only (D) readout condition. Meanwhile, the donor plus acceptor (D/A) readout condition was labeled with both anti-PD-1 (1:100) and rabbit anti-PD-L1 (1:500). The plate was incubated overnight at 4°C before being washed twice with PBS containing 0.02% Tween 20 (PBST). Secondary Fab fragments were added, the D wells were labeled with anti-mouse FabATTO488 (1:100) and the D/A wells labeled with FabATTO488 (1:100) and anti-rabbit FabHRP (1:200). The plate was then incubated for 2 hours at room temperature before being washed twice with PBST and once with PBS.

Tyramide signal amplification was performed on the D/A wells for 20 minutes in the dark, via the addition of Alexa594-conjugated tyramide diluted in amplification buffer (1:100) in the presence of 0.15% H_2O_2 (Supplementary Fig. S2A; Veeriah and colleagues, 2014 and Miles and colleagues, 2017; refs. 19, 20) The D/A wells were washed twice with PBST and once with PBS to remove the tyramide. Prolong diamond antifade mount (5 μL) was added to each well before being mounted with a coverslip.

iFRET assay for CTLA-4/CD80 interaction in cell culture

CTLA-4–expressing Jurkat cells were first seeded onto Millicell 8-well plate, before the blocking antibody, ipilimumab (anti-CTLA-4), was added to four wells at 100 μg/mL final concentration. The CD80–expressing Raji cells were subsequently seeded and incubated for 20 hours at 37°C with 5% CO_2. Unbound cells were removed by PBS washes. The cells were fixed, underwent endogenous peroxidase suppression, and were blocked with BSA as described previously in the PD-1/PD-L1 cell assay. The primary antibodies were added; D wells were labeled with mouse monoclonal anti-CTLA-4 (1:100) and the D/A wells labeled with both anti-CTLA-4 (1:100) and rabbit polyclonal anti-CD80 (1:100). The rest of the protocol was conducted as described above for the PD-1/PD-L1 singe-cell assay.

iFRET assay for PD-1/PD-L1 interaction in FFPE ccRCC tissue

Human ccRCC tissue samples were provided by Cruces University Hospital (Barakaldo, Bizkaia, Spain). Consecutive cross-sections of tissues were mounted on separate slides to allow D and D/A antibody labeling. Samples were obtained from 22 patients, from which, five consecutive tissue section slides were provided. Of the five samples, two were available for D and two for D/A staining, while the remaining section was analyzed using H&E staining to determine regions of immune infiltration.

IHC with PD-L1 (SP-142, Ventana) was performed in Benchmark Ultra (Ventana) Immunostainers following the specific protocol recommended by the manufacturer.

For iFRET sample preparation, antigen retrieval was carried out using Envision Flex solution, pH 9, and a PT-Link Instrument (Dako), where the slides were heated to 95°C for 20 minutes. Remaining paraffin was removed by PBS washes before containing tissue areas with a hydrophobic PAP pen border. One to 2 drops per slide of endogenous peroxidase suppressor were added and the slides were

incubated in a humidified tray for 30 minutes at room temperature. The slides were then blocked with BSA and D slides were labeled with anti-PD-1, while D/A slides were labeled with anti-PD-1 plus anti-PD-L1, following the previously described cell assay protocol.

iFRET assay for PD-1/PD-L1 interaction in FFPE malignant melanoma TMAs

Human malignant melanoma TMAs were provided by Nottingham University Hospital (Nottingham, England, United Kingdom). Consecutive cross-sections of tissues were mounted on separate slides to allow D and D/A antibody labeling. Samples from 176 patients, with two consecutive tissue section slides per patient were provided. Of the two samples, one was available for D and one for D/A staining. The primary antibodies used were anti-PD-1 and anti-PD-L1 following the same protocol as the FFPE RCC tissue above.

iFRET assay for PD-1/PD-L1 interaction in FFPE metastatic NSCLC

Human metastatic NSCLC tissue slices were provided by Institut Bergonié (Bordeaux, France). Consecutive cross-sections of tissues were mounted on separate slides to allow D and D/A antibody labeling. Samples from 40 patients, with two consecutive tissue section slides per patient were provided. Of the two samples, one was available for D and one for D/A staining. The primary antibodies used were anti-PD-1 and anti-PD-L1 following the same protocol as the FFPE ccRCC tissue above.

Statistical analysis

Statistical analysis and box and whisker plots were performed using Origin Pro8. Statistical differences were calculated between groups using the Mann–Whitney *U* test (values indicated on the box and whisker plots). The Mann–Whitney *U* test is a non-parametric test, thus not assuming a normal distribution of results. Box and whisker plots represent the 25%–75% (box) and the 1–99 (whiskers) ranges. Statistical differences are indicated with $P \leq 0.05$. Kaplan–Meier survival analysis was performed using SPSS. SPSS was also used to calculate Cox regression for survival analysis to assess which factors (age, sex, tumor stage, and interaction state) were impacting overall survival. For NSCLC, patients were ranked in order of their FRET efficiency (interaction status) and split into the two groups, those with the lowest 60% of median FRET efficiencies and those with the highest 40%. For melanoma, patients were split into the highest 20% and lowest 80% of FRET efficiencies. To determine these cut-off points for patients with melanoma and NSCLC, maximally selected rank statistics were performed using the R statistical software (version 3.6.2) and the maxstat (version 0.7–25) package, which provides several *P* value approximations (21, 22). Maximally selected rank statistics can be used for estimation as well as evaluation of a simple cut-off point mode. The results provided by maxstat were consistent with the choice of bottom 80% and top 20%, and 60% and 40%, respectively. The log-rank (Mantel–Cox) test was carried out to determine significant differences between the groups.

Results

Development, validation, and benchmarking of a novel amplified FRET imaging assay for determining immune checkpoint interaction in *ex vivo* assays

The iFRET assay used to measure the immune checkpoint interaction state is based on time-resolved FRET. Here, FRET acts as a "chemical ruler," measuring distances of 1–10 nm, which are the same order of magnitude as cell surface interactions. The maximum FRET efficiency value permitted is 50% (Supplementary Materials and Methods). Our definition of interaction is distances under 10 nm, as opposed to proximity ligation assay (PLA), which detects distances of tens of nm and colocalization assays, which range from 100 nm up to 20 μm (Supplementary Fig. S1A; refs. 14, 23).

To develop and validate iFRET for the measurement of immune checkpoint interactions, two antibodies (Promega) were employed; J1201, an experimental antibody for blocking PD-1/PD-L1 interactions, and ipilimumab, for blocking CTLA-4/CD-80 interactions. These antibodies were used to verify iFRET as a technique for detecting the intercellular interaction of these ligand/receptor pairs. These antibodies and cell lines were chosen as they were components from a commercially available validated assay.

Figure 1 illustrates the intercellular interaction of PD-1 and PD-L1, on Jurkat and CHO-K1 cells, using iFRET. Cells were not permeabilized and therefore, the observable interaction was that of two membrane-bound, extracellular proteins. The FLIM images provided in the following figures consist of pseudocolor lifetime maps, which represent lower lifetimes (red) and higher lifetimes (blue). Also provided are grayscale intensity maps, which indicate donor (PD-1 or CTLA-4) expression and acceptor (PD-L1 or CD80) expression. In untreated cells, a lifetime decrease from 1.39 ± 0.11 ns to 1.19 ± 0.12 ns was detected, resulting in a FRET efficiency of 14.38% (**Fig. 1A**). FRET efficiency is correlated to molecular distance; Supplementary Table S3 indicates the range of receptor–ligand distances obtained for the following results. In cells treated with 25 μg/mL of experimental blocking antibody, J1201, the lifetime reduced from 1.35 ± 0.10 ns to 1.29 ± 0.13 ns, yielding a FRET efficiency of 4.44% (**Fig. 1B**). iFRET signal was not observed when either of the primary staining antibody was omitted. Moreover, when each cell type was analyzed alone, no interaction state was detected. The findings indicate that the decrease in donor lifetime reflected by the high FRET efficiency was due to the specific interaction of PD-1 and PD-L1, which was attenuated in the presence of J1201. In both cases, intensity maps confirm the presence of the donor, PD-1 and acceptor, PD-L1. In **Fig. 1C**, a box and whisker plot compares FRET efficiency values in the absence and presence of experimental blocking antibody, J1201 (25 μg/mL). Each point on the graph represents one region of interest, which may contain between five and 25 cells. Mean FRET efficiencies ± SEM are indicated. Mann–Whitney *U* analysis determined statistical differences between treated and untreated cells (**, $P = 0.004$).

Intercellular CTLA-4 and CD80 interactions, in Jurkat and Raji cells, were also assessed using iFRET (**Fig. 2**). Here, in the absence of the blocking antibody, ipilimumab, donor lifetime decreased from 1.96 ± 0.17 ns to 1.45 ± 0.11 ns in the presence of the acceptor. This resulted in a FRET efficiency of 26.02% (**Fig. 2A**). When ipilimumab was added at 100 μg/mL, the donor lifetime decreased from 2.06 ± 0.12 ns to 1.98 ± 0.09 ns, resulting in a FRET efficiency of 3.88% (**Fig. 2B**). Intensity maps confirm the expression of CTLA-4 (donor) and CD-80 (acceptor). Box and whisker plot (**Fig. 2C**) compares FRET efficiency values in the absence and presence of 100 μg/mL ipilimumab. Each point on the graph represents one region of interest, which may contain between five and 25 cells. Mann–Whitney *U* analysis determined statistical differences between treated and untreated cells (***, $P = 3.27 \times 10^{-7}$).

To benchmark the effectiveness of the iFRET assay in clinically relevant settings, we compared the assay with a PLA, which in principle can also visualize PD-1 and PD-L1 within proximities of approximately 40 nm. To achieve this comparison, iFRET and PLA were run on sequential ccRCC tissue sections from the same tissue block. Prior

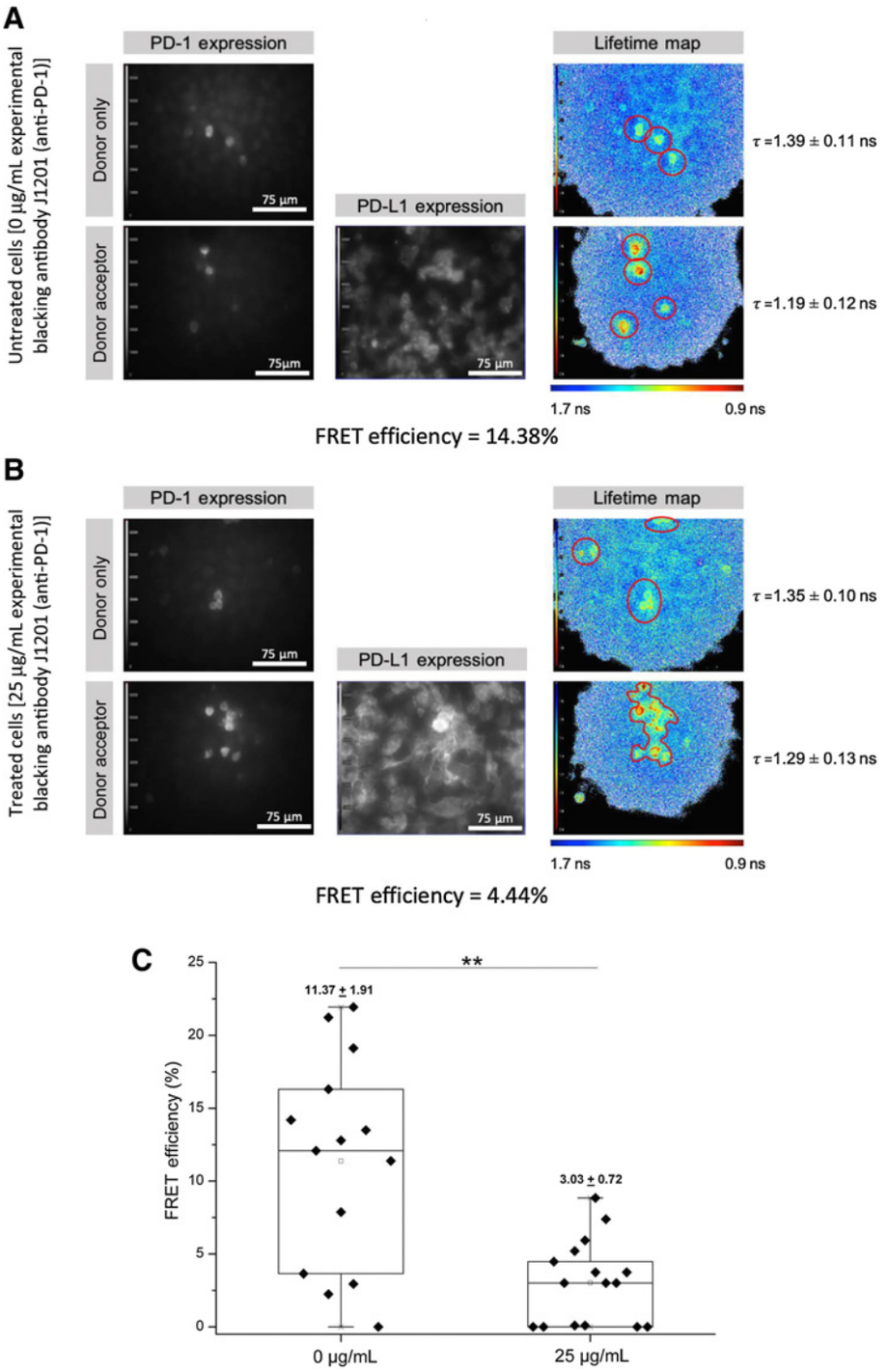

Figure 1.

iFRET detects and quantifies PD-1/PD-L1 interaction between CHO-K1 and Jurkat cells. **A,** FLIM images consist of grayscale expression maps indicating PD-1 expression (donor, ATTO488) and PD-L1 expression (acceptor, ALEXA594). Pseudocolor lifetime maps indicate the lifetime of the donor alone and lifetime of the donor in the presence of the acceptor. A lifetime decrease from 1.39 ± 011 ns to 1.19 ± 0.12 ns yields an FRET efficiency of 14.38% in untreated cells. **B,** When treated with 25 µg/mL J1201 (experimental anti-PD1 blocking antibody), the donor lifetime decreased from 1.35 ± 0.10 ns to 1.29 ± 0.13 ns. This gives an FRET efficiency of 4.44%, indicating a significant reduction of PD-1/PD-L1 interaction. **C,** Box and whisker plot compares FRET efficiency values in the absence and presence of experimental blocking antibody, J1201 (25 µg/mL). Each point on the graph represents one region of interest, which may contain between five and 25 cells. Mean FRET efficiencies ± SEM are indicated. Mann–Whitney *U* analysis determined statistical differences between treated and untreated cells. **, $P = 0.004$.

to the investigation, samples were determined PD-L1 positive (>1%) or negative (<1%) using the Roche VENTANA PD-L1 (SP142) assay.

PLA allowed the qualitative visualization of PD-1 and PD-L1 within close proximity (Supplementary Fig. S3A). The PD-L1–positive ccRCC sample labeled with anti-PD-1, anti-PD-L1, and PLA +/− probes produced measurable PLA signals, albeit comparatively weak signals. Furthermore, PLA signals were observed across both experimental and control groups (normal renal tissue), possibly due to PLA only determining close proximity (up to 40 nm) as opposed to direct interaction (≤10 nm), limiting the specificity of the assay (24).

The box and whisker plots show the interaction states in the PD-L1–positive and PD-L1–negative groups. In the PD-L1–negative group, PLA failed to detect an interaction, whereas iFRET detected two areas of significant interaction (Supplementary Fig. S3B). These observations suggest that iFRET provides greater sensitivity and specificity than PLA, allowing the identification

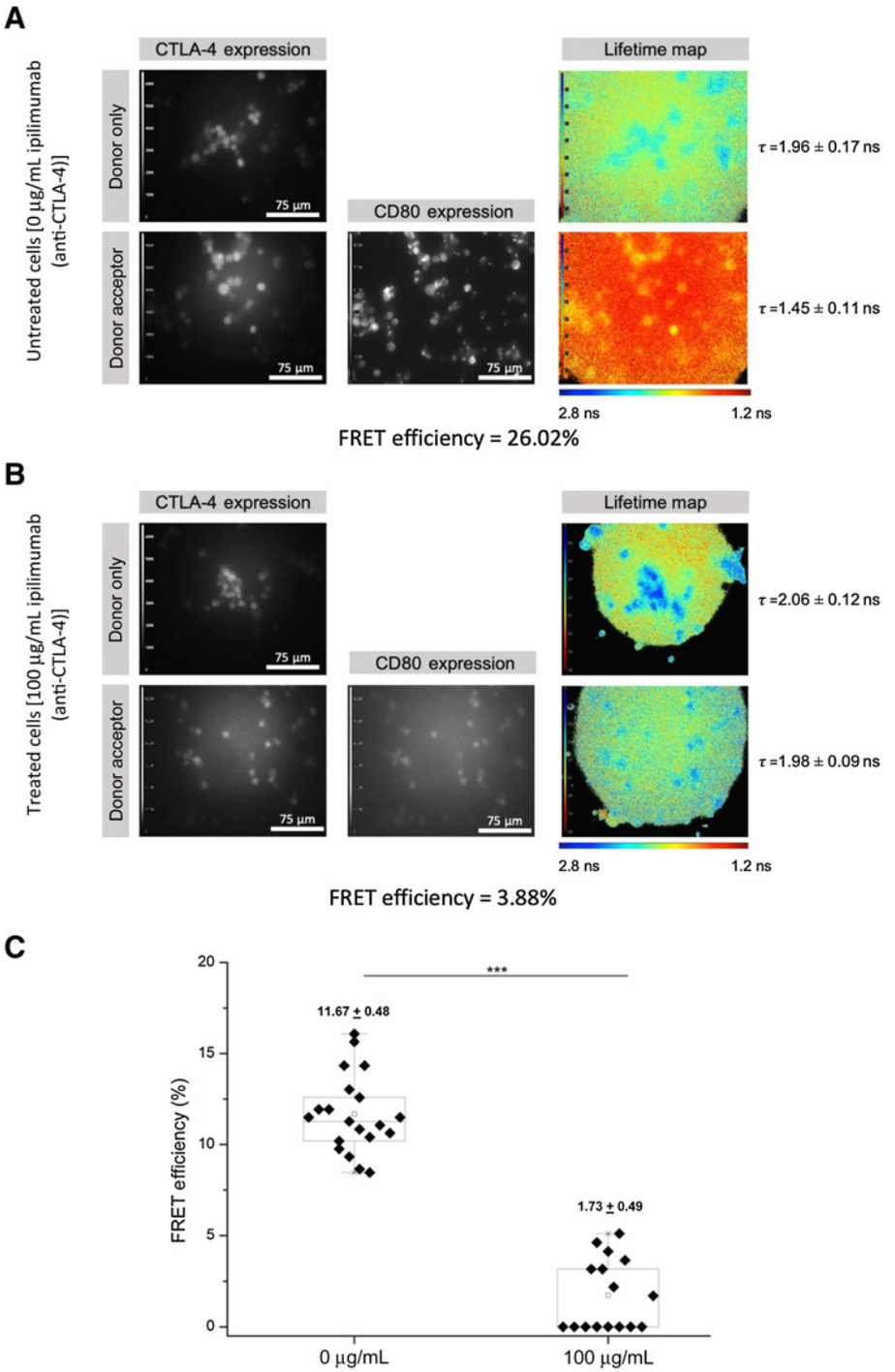

Figure 2.

iFRET precisely determines CTLA-4/CD80 interaction between Raji and Jurkat cells. **A,** In untreated Raji and Jurkat cells, the donor lifetime decreased from 1.96 ± 0.17 ns alone to 1.45 ± 0.11 ns in the presence of the acceptor. This gives an FRET efficiency of 26.02%. **B,** When treated with 100 µg ipilimumab, donor lifetime decreased from 2.06 ± 0.12 ns to 1.98 ± 0.09 ns. This results in an FRET efficiency of 3.88%. **C,** Box and whisker plot compares FRET efficiency values in the absence and presence of 100 µg/mL ipilimumab. Each point on the graph represents one region of interest, which may contain between five and 25 cells. Mann–Whitney *U* analysis determined statistical differences between treated and untreated cells. ***, $P = 3.27 \times 10^{-7}$.

of tumor-mediated immune suppression in patients otherwise considered as PD-L1 negative.

PD-L1 expression does not correspond to interaction status of PD-1 and PD-L1 in ccRCC

Following iFRET optimization and benchmarking, we assessed the interaction of PD-1 and PD-L1 in the subsequent FFPE ccRCC tissue sections from the above cohort of patients with as yet unknown outcomes. The series included samples from 22 patients considered as PD-L1 negative (<1%) or positive (>1%), as determined using the Roche VENTANA PD-L1 (SP142) assay and MSTS. Three regions of interest per patient sample were analyzed and the mean FRET efficiency for each patient was calculated. Across these patients, mean FRET efficiencies varied from 0.17% to 14.1%, indicating iFRET is able to quantitatively detect the heterogeneity of PD-1 and PD-L1 interaction states in patients. **Figure 3A** shows a sample with a donor lifetime decrease from 1.91 ± 0.18 ns to 1.58 ± 0.19 ns. This resulted in a FRET efficiency of 17.28%. Notably, PD-L1 expression, classified by

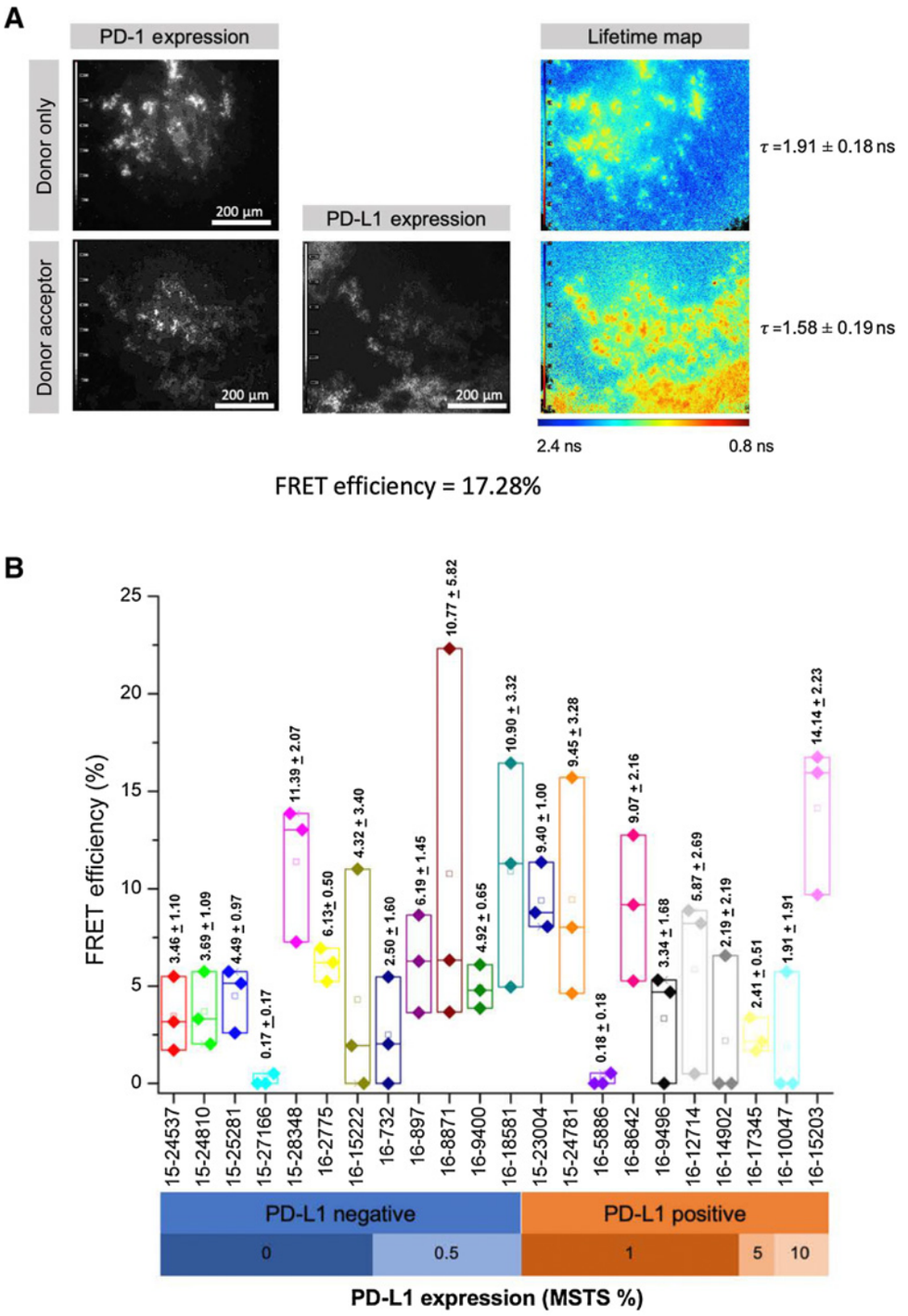

Figure 3.

iFRET detects heterogeneity of PD-1 and PD-L1 interaction in FFPE ccRCC. **A,** Intensity images and lifetime maps (pseudocolor scale) of FFPE human ccRCC patient sample 16-15203. A decrease in donor lifetime from 1.91 ± 0.18 ns alone to 1.58 ± 0.19 ns in the presence of the acceptor gives an FRET efficiency of 17.28%. **B,** Box and whisker plots show the interaction state of each patient in either the PD-L1–negative or PD-1–positive group. Here, iFRET identified that 11 of the 12 PD-L1–negative patients had a significant interaction state. Conversely, one patient in the PD-L1–positive group exhibited no interaction state.

MSTS, did not correlate with the interaction status of PD-1 and PD-L1 as determined by iFRET (**Fig. 3B**). Crucially, iFRET detected significant interaction states in 11 of the 12 PD-L1–negative patients, a functional state that was not detected by conventional IHC methods. Conversely, 1 PD-L1–positive patient showed a minimal interaction state (**Fig. 3B**).

PD-1/PD-L1 interaction state is indicative of patient outcome in malignant melanoma

After analyzing PD-1/PD-L1 interaction in ccRCC tissue, the interaction status in 176 patients with malignant melanoma with known outcomes was assessed. The cohort, which consisted of treated and untreated patients, was predominantly male with a split of 102 males/71 females and a mean age of 66.1 years. Twenty-five percent of patients had stage I tumors, 43.5% had stage II tumors, 9.4% had stage III tumors, and 22.1% had stage IV tumors. Tumor-infiltrating lymphocytes were absent in 39 patients, and 101 patients had focal infiltration with 30 patients experiencing extensive infiltration (Supplementary Table S1). Of the 176 patients, 148 were untreated, 14 received immunotherapies (nivolumab, pembrolizumab, or ipilimumab), and 14 received non-immune therapies (radiotherapy, chemotherapy, or small-molecule inhibitors, e.g., vemurafenib, trametinib, and dabrafenib).

Figure 4A shows the H&E staining of a primary cutaneous malignant melanoma. The panels on the left show the H&E staining of patient 390, a non-ulcerated tumor sample with no tumor-infiltrating lymphocytes, this patient had an FRET efficiency of 3.50%. The top panel shows a ×5 magnification with the lack of ulceration circled, and subsequent ×10 magnifications show the lack of tumor-infiltrating lymphocytes. The panels on the right show patient 131, with high tumor-infiltrating lymphocytes, this patient had an FRET efficiency of 26.20%. The top panel here shows a ×5 magnification indicating the tumor-infiltrating lymphocytes (black circled area) and tumor ulceration (blue circle). The subsequent middle and bottom panels show ×10 magnifications of lymphocyte infiltration and tumor ulceration, respectively. **Figure 4B** shows FLIM images of the sample of patient 390, where intensity maps illustrate the expression of PD-1 and PD-L1. Here, the pseudocolor scale runs from 3.5 ns (blue) to 0.5 ns (red). Despite a high expression of PD-L1 in this patient's sample, a low change in donor lifetime was observed; donor lifetime alone was 1.95 ± 0.16 ns and slightly decreased to 1.88 ± 0.15 ns in the presence of the acceptor. The resulting FRET efficiency was 3.50%. Conversely, **Fig. 4C** shows the sample of patient 131. As observed in the sample of patient 390, patient 131s' sample demonstrated a prominent level of PD-L1 expression. However, unlike patient 390, patient 131 displayed a high interaction state between ligand and receptor, with the donor lifetime decreasing from 2.22 ± 0.19 ns to 1.64 ± 0.15 ns when in the presence of the acceptor, with a resulting FRET efficiency of 26.20%. These results reinforce the hypothesis that PD-L1 expression does not correlate with PD-1/PD-L1 interaction.

The interaction state was assessed with respect to clinical PD-L1 expression scores for 159 of the 176 patients in this cohort (PD-L1 scores were not available for the remaining 17 patients). **Figure 5A** shows the lack of correlation between clinical PD-L1 expression scores and interaction state determined by iFRET. Here, the clinical IHC images of patient 390 (bottom) and patient 131 (top) are shown. As this was performed on a TMA, each patient had one FRET efficiency value, with each point of the box and whisker plot representing one patients' FRET efficiency. Of the 117 patients who were stratified as being PD-L1 negative, 58 showed a PD-1/PD-L1 interaction state; a functional state not detected by conventional IHC methods. Of the 42 patients who were in the PD-L1–positive group, 19 showed no interaction despite the presence of the ligand.

We then correlated PD-1/PD-L1 interaction state with patient survival. The cohorts were ranked in order of their FRET efficiency values and sorted into the following categories: those with the lowest 80% of FRET efficiencies and those with the highest 20%. In **Fig. 5B**, Kaplan–Meier survival analysis revealed that those with the lowest 80% of FRET efficiencies had a significantly worse outcome than those with the highest 20% (log-rank Mantel–Cox, $P = 0.05$). Cox regression for survival analysis revealed PD-1/PD-L1 interaction was the only significant factor impacting overall survival ($P = 0.019$). We then sought to apply Kaplan–Meier analysis to correlate the clinical PD-L1 scores with patient outcome. In **Fig. 5C**, there is no significant difference in outcome between the PD-L1–positive and PD-L1–negative patients (log-rank Mantel–Cox, $P = 0.87$). This illustrates that iFRET is more informative on patient outcome than conventional IHC approaches reporting ligand expression.

Lower PD-1/PD-L1 interaction states correlate with worsened overall and progression-free survival in metastatic NSCLC

Next, in an outcome blinded study, we applied iFRET to samples from patients with metastatic NSCLC. A statistical power calculation indicated that, to obtain results with at least 80% significance, a sample number of >30 was required, hence we tested 60 FFPE samples, all from anti-PD-1 posttreatment patients. Of these 60 patients, 40 had clinical follow-up and outcome and were used to create Kaplan–Meier survival plots. The cohort comprised of 36 males and 24 females with an age range of 44–86 years (median age, 63 years; Supplementary Table S2). Performance status was defined, and 50 patients had a performance status of ≤1 and 10 patients had a status of ≥1 (see Materials and Methods).

Pathologist assessment highlighted regions of interest within each sample by identifying tumors and regions of immune cell infiltration for each sample. To analyze the whole region of interest within a patient sample, multiple subregions were analyzed for PD-1/PD-L1 interaction state, resulting in a range of FRET efficiencies for each patient. **Figure 6A** shows FLIM images demonstrating that as in other tumor settings (see above), PD-1 and PD-L1 expression levels do not correlate with interaction state. The pseudocolor scale (ranging from 1.0 ns to 2.7 ns) illustrates a donor lifetime decrease from 1.99 ± 0.17 ns to 1.44 ± 0.14 ns yielding an FRET efficiency of 27.64%. **Figure 6B** is a box and whisker plot, where each plot represents 1 patient. Each plot represents all the FRET efficiency values obtained for each patient, with the median value written above each plot. The highest median FRET efficiency value was 29.90% and the lowest being 0.00%. The box and whisker diagram demonstrates the ability of iFRET to quantify inter- and intrapatient heterogeneity of PD-1/PD-L1 interactions in metastatic NSCLC (**Fig. 6B**).

The survival data of 40 patients were subsequently analyzed and correlated to each patient's FRET efficiency, indicating their PD-1/PD-L1 interaction state. Patients were then ranked in order of their median FRET efficiency and split into the following two groups: those with the highest 40% of median FRET efficiencies and those with the lowest 60% of median FRET efficiencies. Kaplan–Meier survival analysis demonstrated that for these anti-PD-1–treated patients, those with the lowest 60% median FRET efficiency values, and therefore, a lower PD-1/PD-L1 interaction state, had a significant worsened overall survival ($P = 0.05$; **Fig. 7A**). When analyzing PD-L1 expression (indicated by acceptor intensity), Kaplan–Meier analysis failed to determine a difference between those with a high PD-L1 expression

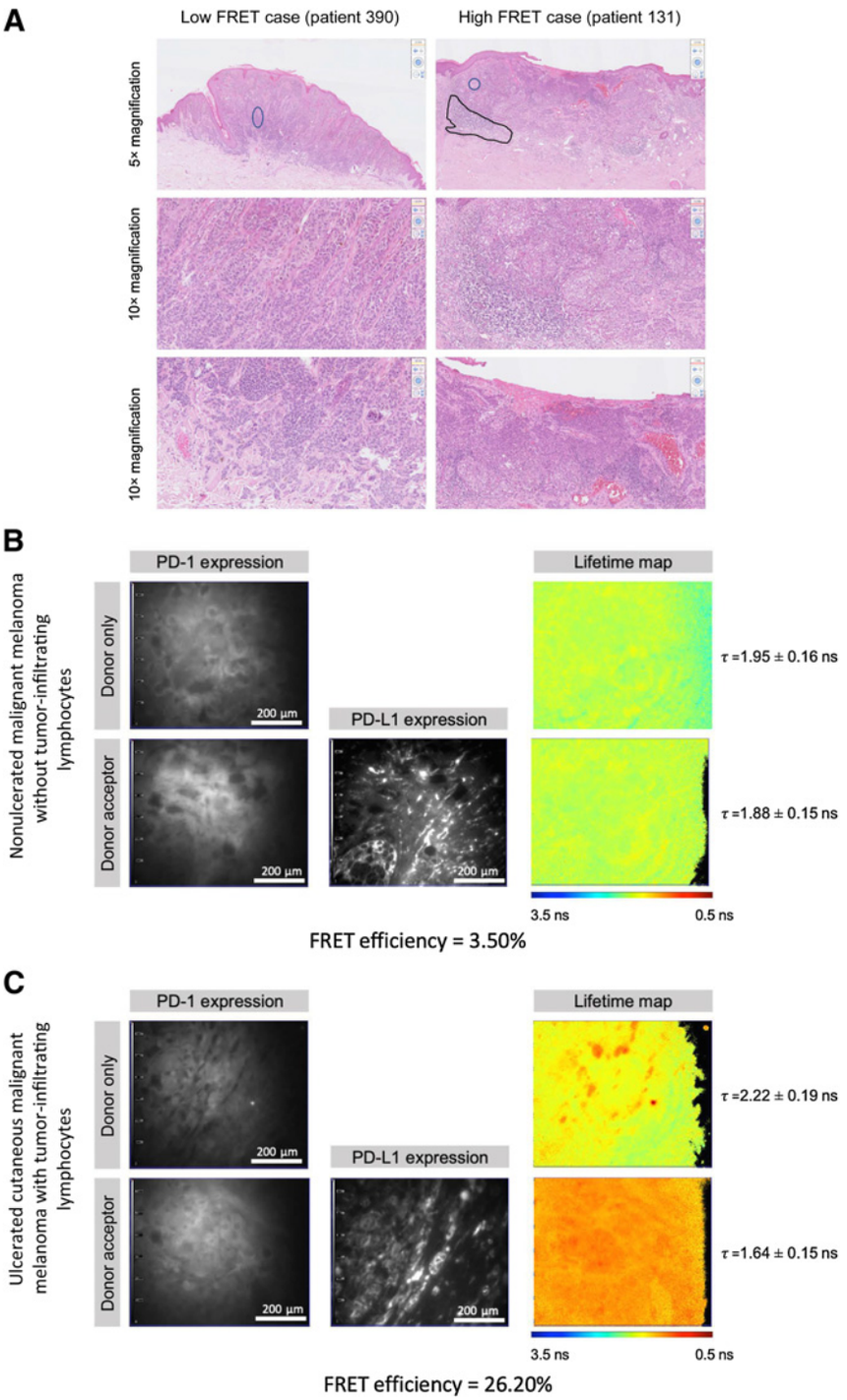

Figure 4.

PD-L1 expression does not correlate with PD-1/PD-L1 interaction state in malignant melanoma. **A,** The H&E staining of the sample of patient 390 with an FRET efficiency of 3.50% (left). A scanning view of the non-ulcerated (blue circle) tumor at ×5 magnification, with the subsequent images showing high power (magnification, ×10) images of the tumor, highlighting a lack of tumor-infiltrating leukocytes (top). The H&E staining of patient 131 with an FRET efficiency of 26.20% (right). A scanning view of the tumor with the tumor-infiltrating leukocytes shown (black marked area) and tumor ulceration (blue circle; top). Tumor leukocyte infiltration (middle) and tumor ulceration (bottom) at a magnification of ×10. **B,** FLIM images show a melanoma with a low PD-1/PD-L1 interaction state. Expression images, based on PD-1 or PD-L1 intensity, show the presence of the receptor and ligand, however, the lifetime map shows no change in pseudocolor, indicating a lifetime change from 1.95 ± 0.16 ns to 1.88 ± 0.15 ns and thus, no interaction state. **C,** FLIM images show a melanoma sample with a high PD-1/PD-L1 interaction state. Again, the expression maps show the presence of PD-1 and PD-L1 as in **B**, however, the change in pseudocolor represents a change in lifetime from 2.22 ± 0.19 ns to 1.64 ± 0.15 ns, indicating a high interaction state.

and those with a low PD-L1 expression ($P = 0.97$; **Fig. 7B**). This again shows the shortcomings of using PD-L1 expression levels to determine patient outcome.

Discussion

This study has demonstrated the application of iFRET to detect intercellular ligand–receptor interactions. The method combines a two-site, time-resolved FRET assay and signal amplification, with a tissue preparation time identical to that of IHC approaches. The high-throughput frequency domain FRET/FLIM imaging platform allowed mapping and automated acquisition of data from both cell cultures and arrayed tissue samples, thereby creating a straightforward procedure for non-specialized personnel (Supplementary Materials and Methods). The automatic detection of regions of interest within the acquisition process significantly reduced operator bias.

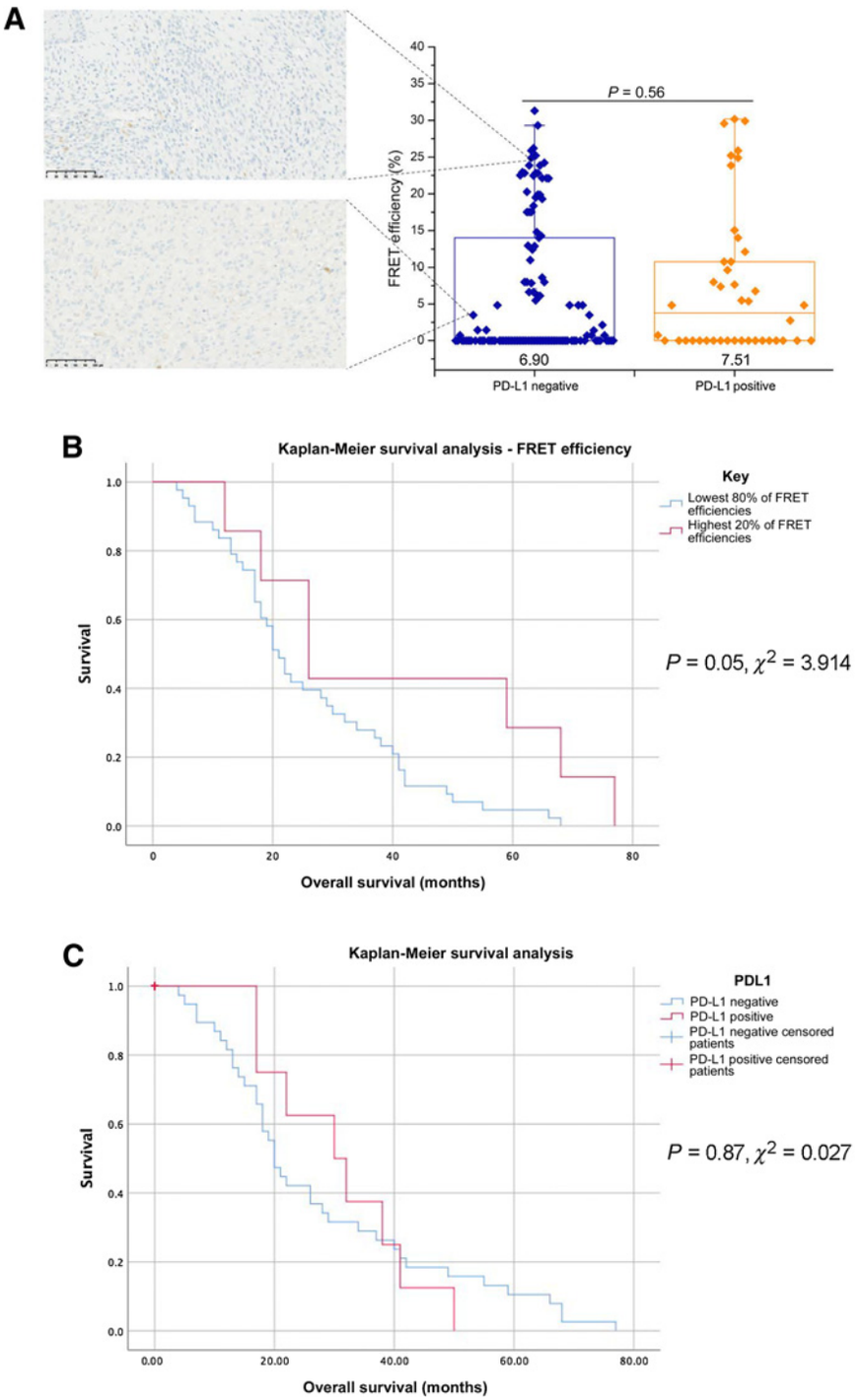

Figure 5.

PD-1/PD-L1 interaction state predicts patient outcome in malignant melanoma, where PD-L1 expression fails to do so. **A,** PD-L1 was labeled and patients' clinical PD-L1 expressions were determined as PD-L1 negative or PD-L1 positive. PD-L1 expression status was correlated with interaction state. Within the patients' assessed as PD-L1 negative, iFRET determined 58 patients that showed an interaction state, with 59 patients in the PD-L1–negative group showing no interaction state. Conversely, in those patients clinically stratified as PD-L1 positive, iFRET determined that 19 of 42 patients showed no interaction state. The IHC PD-L1 images of patients 390 and 131 with FRET efficiencies of 3.50% and 26.2%, respectively, are shown. **B,** Kaplan–Meier survival analyses comparing patients with the highest 20% of FRET efficiencies and those with the lowest 80% ($n = 176$). Those with a lower PD-1/PD-L1 interaction state (lower FRET efficiency) had an improved overall survival compared with those with a higher interaction state (log-rank Mantel–Cox, $P = 0.05$), underpinning the ability of iFRET to predict patient outcome. **C,** Clinical PD-L1 scores defined patients as being PD-L1 positive or PD-L1 negative. Kaplan–Meier analysis detected no significant difference in patient outcome when correlated with PD-L1 expression (log-rank Mantel–Cox, $P = 0.87$), exhibiting that PD-L1 expression levels fail to predict patient outcome.

This assay measures receptor–ligand distances of 1–10 nm and determines interaction as any distance that falls within this range. Currently, alternative assays have utilized PD-1 and PD-L1 expression to determine receptor–ligand proximity. Tumeh and colleagues, 2014, have applied an assay that determines the presence of PD-1 and PD-L1 in close proximity to be an interaction (25). However, the working distances of intensity colocalization assays are far greater (70 nm–20 μm) than that of iFRET. Moreover, when expression readouts were used in the pathologies assessed here, PD-L1 expression did not correlate with interaction state or patient outcome.

The iFRET methodology was exemplified for assessing the interaction status of two immune checkpoint pairs, PD-1/PD-L1 and CTLA-4/CD80, in single-cell assays and biopsy tissue samples from patients with ccRCC, primary malignant melanoma, and metastatic

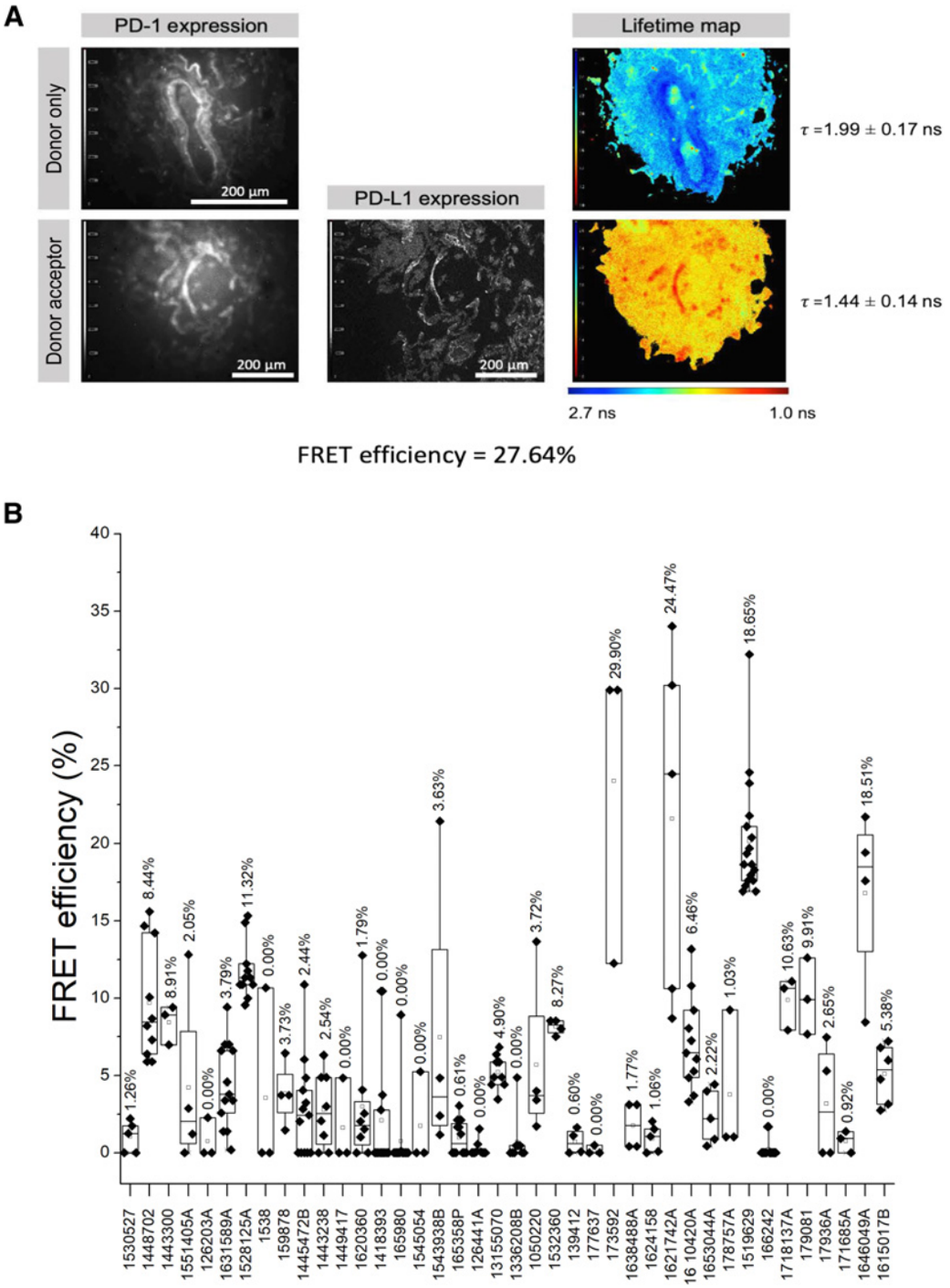

Figure 6.

iFRET quantifies PD-1/PD-L1 interaction state in metastatic NSCLC alongside inter- and intrapatient heterogeneity. **A,** FLIM images show intensity and lifetime maps of a FFPE metastatic NSCLC sample. Intensity images show PD-1 and PD-L1 expressions, respectively. The pseudocolor scale illustrates a donor lifetime decrease from 1.99 ± 0.17 ns to 1.44 ± 0.14 ns, yielding an FRET efficiency of 27.64%. **B,** Box and whisker plots quantify the interaction states observed, with each plot representing the interaction states detected within each patient sample. Values above each plot represent the median FRET efficiency value for each patient sample. The highest median FRET efficiency value observed was 29.90% and the lowest 0.00%. iFRET not only quantifies interpatient heterogeneity but also intrapatient heterogeneity.

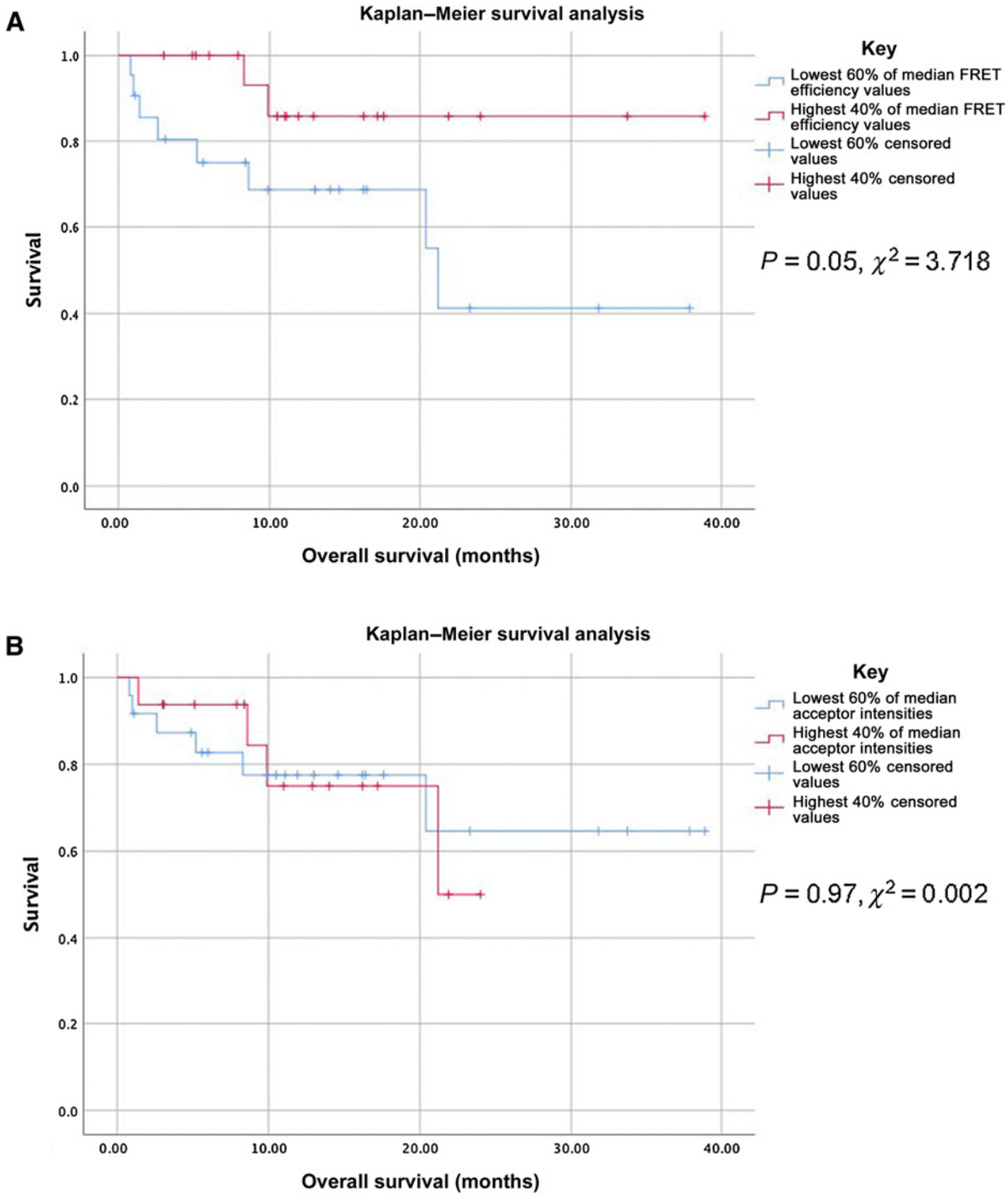

Figure 7.

Lower PD-1/PD-L1 interaction correlates to a significantly worsened patient survival in metastatic NSCLC. **A,** Anti-PD-1 post-treatment patients were ranked by their mean FRET efficiency value and grouped into the following: the lowest 60% of median FRET efficiencies and the highest 40% of median FRET efficiencies. Those with the lowest 60% of median FRET efficiencies had a significantly ($P = 0.05$) worsened overall survival. **B,** Patients were ranked by their PD-L1 expression (acceptor intensity) and split into the lowest 60% of median acceptor intensities and the highest 40%. Kaplan–Meier survival analysis was unable to detect a difference between the two groups (log-rank Mantel–Cox, $P = 0.97$).

NSCLC. The initial validation of the method in single-cell coculture assays, where manipulation of ligand–receptor interactions can be specifically suppressed, has provided the confidence to assess these complexes in patient biopsies. The additional controls with respect to the use of secondary labeled reagents only, without the presence of primary antibodies, adds further control to this two-site assay.

Comparison of iFRET with PLA provided evidence that the latter did not perform as well in these settings in identifying interaction. By its very design, the iFRET methodology elaborated here provides both a measure of ligand–receptor interaction and the spatial resolution of this interaction. Importantly, this is readily achieved in routinely fixed samples from patient biopsies, offering great promise in being able to inform on the more detailed behavior of these interactions and their distribution within pathologic settings. This is well illustrated here with the observed heterogeneity seen not simply between patient biopsies, but within individual biopsies reflected in the spread of FRET efficiencies across regions of interest for individual patients. This heterogeneity may reflect differential patterns of reprogramming of the tumor microenvironment playing out in modified immune suppressive ligand presentation and/or variability in the degree of immune cell infiltration.

A lack of correlation between the extent of PD-1/PD-L1 interaction state and the expression levels of these two proteins was evident in ccRCC, malignant melanoma, and metastatic NSCLC cohorts. In both melanoma and NSCLC, it was shown that PD-L1 expression levels were unable to predict patient outcome. This questions current protocols that rely on IHC PD-L1 expression levels to predict patient outcome and, thus, have implications for the use of simple expression levels to stratify patients for treatment. Moreover, in patients with ccRCC, high interaction states were observed in patients who would otherwise be labeled as PD-L1 negative. Blockade of interaction would be predicted to be effective in contexts where elevated levels of interaction occur and is by inference responsible for the immune privileged state of the tumor. Hence, interaction would *a priori* be a criterion for treatment.

To examine the potential impact of this approach further, a unique cohort of patients with metastatic NSCLC was studied. The cohort of patients from which the FFPE samples were derived were all treated with anti-PD-1 monotherapies and had full clinical follow-up and outcomes. Within this cohort, iFRET has shown the potential for a high versus low PD-1/PD-L1 interaction state to be utilized as a predictive clinical biomarker posttreatment. Conceptually, it is surmised that a high degree of PD-1/PD-L1 interaction infers tumor selection in patients, indicating that the patient's tumor may be reliant on PD-1/PD-L1 interaction to facilitate immune evasion. It is precisely this group of patients that would be expected to respond to immune checkpoint inhibition.

As these were post-treatment samples from responsive patients with metastatic NSCLC, it was questioned why a high level of PD-1/PD-L1 interaction state might be observed? The pharmacodynamics of immune checkpoint disruption as a measure of target interaction have not been monitored to date. As such, it is not known whether blockade of checkpoint interaction needs to be either sustained or complete. The working hypothesis derived from this dataset is that interaction is likely incomplete and as such, a threshold level of T-lymphocyte complex disengagement is sufficient to trigger the observed responses to intervention. It will be informative in a suitable setting to monitor complex disengagement as a function of time following treatment.

Those patients with low interaction and therefore, worsened survival may nevertheless benefit from alternative immune therapies. These tumors may evade the immune system by dysregulating CTLA-4/CD80 or other inhibitory interactions. Furthermore, no tumor will discretely dysregulate one pathway, in fact, a tumor may evolve to evade host immune response by modulating multiple pathways simultaneously, indicating a patient group who would benefit from dual checkpoint inhibitor therapies (26, 27).

iFRET can be exploited to monitor other intercellular protein interactions and there are ongoing developments designed to capture related immune modulatory interactions pertinent to cancer and emerging cancer treatments. This provides the potential for iFRET to become a useful predictive tool informing on the nature of the tumor immune-privileged state. While single-region analysis has here provided insight into treatment responses, multiregional analysis may provide a more comprehensive view. Furthermore, as a principle, it is clear that this approach has capabilities beyond immune–tumor cell interactions and the broader uptake of the approach promises to be informative in many research (e.g., axon guidance) and clinical (e.g., angiopathies) settings.

The exemplification of iFRET in tumor settings opens up exciting and powerful new opportunities to move beyond the cataloguing of cell phenotypes *in situ* and add functional attributes to our patient data inventory, impacting clinical decisions. This is a routine parameter for small-molecule inhibitors targeted at driver mutations, and we suggest it should become a routine for these more complex biotherapeutic interventions.

Disclosure of Potential Conflicts of Interest

B. Larijani reports a patent for international (PCT) patent application no. PCT/EP2018/062719 "Kits, methods, and their uses for detecting cell–cell interactions." B. Larijani also reports the patent PCT/GB14/050715 "TSA amplification in FRET/FLIM." As disclosed upon submission of the article for peer-review, B. Larijani is a co-founder of FASTBASE Solutions. The conflicts of interests are related to the interpretation of the clinical data. They have been and will be managed in the following manner: The iFRET platform was developed so that it could provide unbiased acquisition and interpretation of data. Hence, it was automated in a specific manner that the operator would not be making biased decisions. Moreover, all the patient samples are blinded during both acquisitions and interpretation of data. The parameters were revealed to us once we had completed the acquisition and interpretation of the data. R. Mehta reports non-financial support from FASTBASE Solutions (shareholder and advisor) outside the submitted work, as well as has a patent for WO2018210927 pending. A. Italiano reports grants and personal fees from Bayer and Roche, grants from MSD and BMS, and personal fees from Springworks outside the submitted work. P.J. Parker reports being a co-founder and shareholder of FASTBASE Solutions S.L. outside the submitted work and has a patent for amplified FRET issued and licensed to FASTBASE Solutions and a patent for iFRET pending (FASTBASE license). No potential conflicts of interest were disclosed by the other authors.

Authors' Contributions

L. Sánchez-Magraner: Conceptualization, data curation, methodology. **J. Miles:** Data curation, formal analysis, investigation, methodology, writing-original draft, writing-review and editing. **C.L. Baker:** Data curation, methodology. **C.J. Applebee:** Data curation, methodology. **D.-J. Lee:** Data curation. **S. Elsheikh:** Resources, data curation. **S. Lashin:** Data curation. **K. Withers:** Data curation. **A.G. Watts:** Resources. **R. Parry:** Resources. **C. Edmead:** Writing-review and editing. **J.I. Lopez:** Resources, data curation. **R. Mehta:** Conceptualization. **A. Italiano:** Resources, data curation. **S.G. Ward:** Formal analysis, writing-review and editing. **P.J. Parker:** Conceptualization, validation, methodology, writing-review and editing. **B. Larijani:** Conceptualization, data curation, supervision, validation, methodology, project administration, writing-review and editing.

Acknowledgments

This work was supported, in part, by Department of Education, Basque Government- IT1270-19, Elkartek grant (BG18), and the Spanish Ministry grant (MINECO) PROJECTS of EXCELLENCE (BFU2015-65625-P). P.J. Parker was supported by a core grant to the Francis Crick Institute, from Cancer Research UK (FC001130), the UK Medical Research Council (FC001130), and the Wellcome Trust (FC001130). We would like to thank Pierre Leboucher for the automation of the multiple frequency domain FLIM and Patel Poulam, clinical oncologist at Nottingham, for clinical discussions. We would also like to thank Audrey Colomba at the Francis Crick Institute for her help in PLA image acquisition.

The costs of publication of this article were defrayed in part by the payment of page charges. This article must therefore be hereby marked *advertisement* in accordance with 18 U.S.C. Section 1734 solely to indicate this fact.

Received April 7, 2020; revised June 15, 2020; accepted August 7, 2020; published first August 27, 2020.

References

1. Hanahan D, Weinberg RA. Biological hallmarks of cancer. In Holland-Frei Cancer Medicine, Ninth Edition, Bast RC, et al., editors. Hoboken, New Jersey: Wiley-Blackwell, 2017. p. 646–74.
2. Pardoll DM. The blockade of immune checkpoints in cancer immunotherapy. Nat Rev Cancer 2012;12:252–64.
3. Alsaab HO, Sau S, Alzhrani R, Tatiparti K, Bhise K, Kashaw SK, et al. PD-1 and PD-L1 checkpoint signaling inhibition for cancer immunotherapy: mechanism, combinations, and clinical outcome. Front Pharmacol 2017;8:561.
4. Engelhardt JJ, Sullivan TJ, Allison JP. CTLA-4 overexpression inhibits T cell responses through a CD28-B7-dependent mechanism. J Immunol 2006;177: 1052–61.
5. Okazaki T, Honjo T. The PD-1-PD-L pathway in immunological tolerance. Trends Immunol 2006;27:195–201.
6. Mahmoudi M, Farokhzad OC. Cancer immunotherapy: wound-bound checkpoint blockade. Nat Biomed Eng 2017;1:0031.
7. Ross K, Jones RJ. Immune checkpoint inhibitors in renal cell carcinoma. Clin Sci 2017;131:2627–42.
8. Heidegger I, Pircher A, Pichler R. Targeting the tumor microenvironment in renal cell cancer biology and therapy. Front Oncol 2019;9:490.
9. Qin S, Xu L, Yi M, Yu S, Wu K, Luo S. Novel immune checkpoint targets: moving beyond PD-1 and CTLA-4. Mol Cancer 2019;18:155.
10. Sommer U, Eckstein M, Ammann J, Braunschweig T, Macher-Goppinger S, Schwamborn K, et al. Multicentric analytical and inter-observer comparability of four clinically developed programmed death-ligand 1 immunohistochemistry assays in advanced clear-cell renal cell carcinoma. Clin Genitourin Cancer 2020 Feb 15 [Epub ahead of print]. DOI: 10.1016/j.clgc.2020.02.009.
11. Theelen W, Baas P. Pembrolizumab monotherapy for PD-L1 >/=50% non-small cell lung cancer, undisputed first choice? Ann Transl Med 2019;7:S140.
12. Roach C, Zhang N, Corigliano E, Jansson M, Toland G, Ponto G, et al. Development of a companion diagnostic PD-L1 immunohistochemistry assay for pembrolizumab therapy in non-small-cell lung cancer. Appl Immunohistochem Mol Morphol 2016;24:392–7.
13. Nunes-Xavier CE, Angulo JC, Pulido R, López JI. A critical insight into the clinical translation of PD-1/PD-L1 blockade therapy in clear cell renal cell carcinoma. Current Urology Reports 2019;20:1.
14. Giraldo NA, Nguyen P, Engle EL, Kaunitz GJ, Cottrell TR, Berry S, et al. Multidimensional, quantitative assessment of PD-1/PD-L1 expression in patients with Merkel cell carcinoma and association with response to pembrolizumab. J Immunother Cancer 2018;6:99.
15. Johnson DB, Bordeaux J, Kim JY, Vaupel C, Rimm DL, Ho TH, et al. Quantitative spatial profiling of PD-1/PD-L1 interaction and HLA-DR/IDO-1 predicts improved outcomes of anti-PD-1 therapies in metastatic melanoma. Clin Cancer Res 2018;24:5250–60.
16. Delahunt B, Cheville JC, Martignoni G, Humphrey PA, Magi-Galluzzi C, McKenney J, et al. The International Society of Urological Pathology (ISUP) grading system for renal cell carcinoma and other prognostic parameters. Am J Surg Pathol 2013;37:1490–504.
17. Lopez JI, Cortes JM. Multisite tumor sampling: a new tumor selection method to enhance intratumor heterogeneity detection. Hum Pathol 2017;64:1–6.
18. Oken MM, Creech RH, Tormey DC, Horton J, Davis TE, McFadden ET, et al. Toxicity and response criteria of the Eastern Cooperative Oncology Group. Am J Clin Oncol 1982;5:649–55.
19. Veeriah S, Leboucher P, de Naurois J, Jethwa N, Nye E, Bunting T, et al. High-throughput time-resolved FRET reveals Akt/PKB activation as a poor prognostic marker in breast cancer. Cancer Res 2014;74:4983–95.
20. Miles J, Applebee CJ, Leboucher P, Lopez-Fernandez S, Lee DJ, Guarch R, et al. Time resolved amplified FRET identifies protein kinase B activation state as a marker for poor prognosis in clear cell renal cell carcinoma. BBA Clin 2017; 8:97–102.
21. Lausen B, Schumacher M. Maximally selected rank statistics. Biometrics 1992;48: 73–85.
22. Hothorn T, Lausen B. On the exact distribution of maximally selected rank statistics. Comput Stat Data Anal 2003;43:121–37.
23. Söderberg O, Leuchowius KJ, Gullberg M, Jarvius M, Weibrecht I, Larsson LG, et al. Characterizing proteins and their interactions in cells and tissues using the *in situ* proximity ligation assay. Methods 2008;45:227–32.
24. Debaize L, Jakobczyk H, Rio AG, Gandemer V, Troadec MB. Optimization of proximity ligation assay (PLA) for detection of protein interactions and fusion proteins in non-adherent cells: application to pre-B lymphocytes. Mol Cytogenet 2017;10:27.
25. Tumeh PC, Harview CL, Yearley JH, Shintaku IP, Taylor EJ, Robert L, et al. PD-1 blockade induces responses by inhibiting adaptive immune resistance. Nature 2014;515:568–71.
26. Autio KA, Boni V, Humphrey RW, Naing A. Probody therapeutics: an emerging class of therapies designed to enhance on-target effects with reduced off-tumor toxicity for use in immuno-oncology. Clin Cancer Res 2020:26.
27. Intlekofer AM, Thompson CB. At the bench: preclinical rationale for CTLA-4 and PD-1 blockade as cancer immunotherapy. J Leukoc Biol 2013;94:25–39.